

# Non-linear modeling of the Edge Localized Mode control by Resonant Magnetic Perturbations in ASDEX Upgrade

F.Orain<sup>1</sup>, M.Hözl<sup>1</sup>, E.Viezzer<sup>1</sup>, M.Dunne<sup>1</sup>, M.Bécoulet<sup>2</sup>, P.Cahyna<sup>3</sup>, G.T.A.Huijsmans<sup>2</sup>, M.Willensdorfer<sup>1</sup>, W.Suttrop<sup>1</sup>, A.Kirk<sup>4</sup>, S.Pamela<sup>4</sup>, S.Günter<sup>1</sup>, K.Lackner<sup>1</sup>, E.Strumberger<sup>1</sup>, A.Lessig<sup>1</sup>, M.Faitsch<sup>1</sup>, the ASDEX Upgrade Team<sup>1</sup> and the EUROfusion MST1 Team<sup>\*</sup>

<sup>1</sup>*Max-Planck-Institut für Plasmaphysik, Garching, Germany*

<sup>2</sup>*CEA, IRFM, 13108 Saint-Paul-Lez-Durance, France*

<sup>3</sup>*Institute of Plasma Physics of the CAS, Prague, Czech Republic*

<sup>4</sup>*CCFE, Culham Science Centre, OX14 3DB, UK*

<sup>\*</sup>*See appendix of H. Meyer et.al. (OV/P-12) Proc. 26th IAEA FEC 2016, Kyoto, Japan*

*Corresponding Author: forain@ipp.mpg.de*

## Abstract:

The plasma response to Resonant Magnetic Perturbations (RMPs) and the interplay between Edge Localized Modes (ELMs) and RMPs is modeled with the non-linear resistive MHD code JOREK, using data from ASDEX Upgrade experimental discharges. The RMP spectrum leading to a maximum amplification of edge kink modes also induce the largest resonant response due to poloidal coupling between modes. In this case, the toroidal coupling between ELMs and RMPs prevents the higher  $n$  modes to grow into a large ELM. However when the plasma response to RMPs is minimum, the RMP drive is not strong enough to affect the growth of the ELMs.

## 1 Introduction

Edge Localized Modes (ELMs) are instabilities occurring in the high confinement (H-mode) regime at the edge of tokamak plasmas. They are characterized by quasiperiodic bursts expelled from the plasma, generating large heat loads on the divertor. In ITER, the predicted heat loads induced by ELMs may be intolerable for the materials, thus ELM mitigation techniques must be developed. One of the foreseen methods is the application of non-axisymmetric Resonant Magnetic Perturbations (RMPs), already proven capable of mitigating or suppressing the ELMs in current tokamak devices [1-6]. Even though the understanding of the impact of RMPs on ELM plasmas has been improved in the last years [7-12], important uncertainties must be overcome to give reliable predictions for ITER. In particular the different parameters governing the plasma response to RMPs as well as the interaction of ELMs with RMPs remain unclear.

The “resonant response” (formation of magnetic island chains on resonant surfaces – estimated particularly important at the pedestal top – and of an ergodic layer at the plasma edge) was first identified to be a key for the ELM mitigation, but the “kink response” (excitation of a barely stable kink mode by RMPs at the plasma edge) was recently shown to play a major role as well [10]. This work aims at assessing the role that

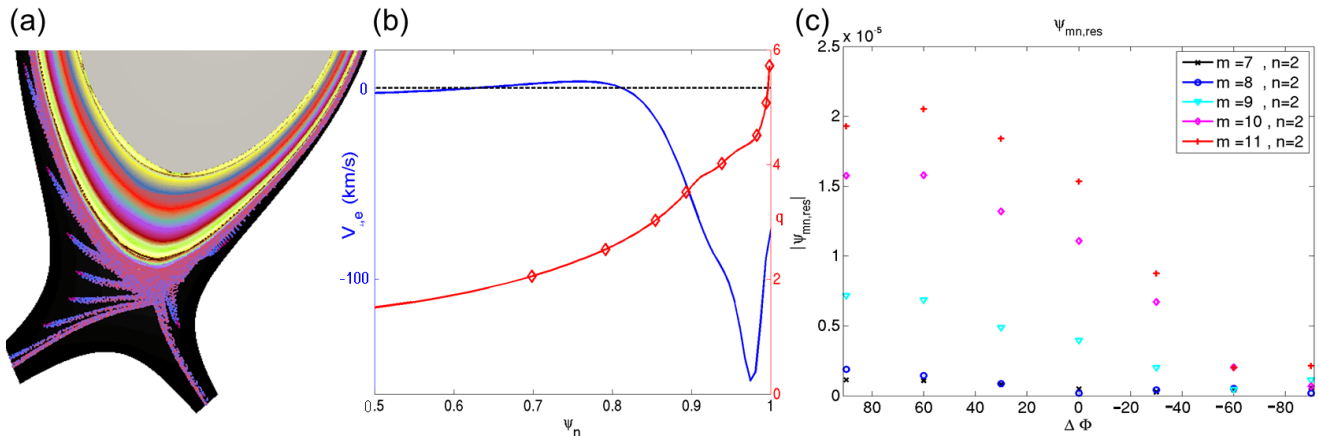


FIG. 1: (a) Poincaré plot of the magnetic topology in the  $\Delta\Phi = -90^\circ$  case. (b) Radial profile of the electron perpendicular velocity (blue) and  $q$ -profile highlighting the position of resonant surfaces  $q = m/2$ . (c) Magnetic flux perturbation on the resonant surfaces depending on the phase  $\Delta\Phi$  between coil currents.

both the resonant response and the kink response have on the ELM mitigation, in order to move towards a more quantitative understanding of current experiments and better predictive capabilities for future experiments.

## 2 Modeling of the RMP effect on ASDEX Upgrade plasmas and comparison to experiments

Non-linear resistive MHD simulations were performed with the JOREK code [13], using input equilibrium profiles and an RMP spectrum closely matching the experimental data of ASDEX Upgrade shots at low collisionality [12]. The JOREK model used evolves in time the reduced MHD equations; toroidal rotation source, two-fluid diamagnetic effects and neoclassical friction allow for a good agreement of the modeled equilibrium plasma flows with the measured rotation [14-15]. RMP fields calculated with the VACFIELD code [16] are applied as boundary conditions at the edge of the JOREK computational domain (covering main plasma and Scrape-Off Layer). The experimental RMP coil amplitude and configurations ( $n = 2$  toroidal mode number, poloidal mode spectrum  $m$  varied by means of differential phase  $\Delta\Phi$  between upper and lower coil currents) are used in modeling.

The interaction between  $n = 2$  RMPs and plasma flows is first considered without ELMs: only the interaction between  $n = 2$  RMPs and plasma flows is considered in this section. Equilibrium reconstruction of H-mode discharges #31128 and #30826 are used as input for modeling (shots with similar plasma parameters but the phase  $\Delta\Phi$  – ie the applied RMP poloidal spectrum – is scanned between  $+90^\circ$  and  $-90^\circ$  in shot #31128, while the phase is kept constant to  $+90^\circ$  in shot #30826 [12]). For  $\Delta\Phi = +90^\circ$ , the ELM frequency is most reduced in the experiment; for  $\Delta\Phi = -90^\circ$ , a transient ELM-free phase is observed leading to density increase terminated by large ELM activity [12]. In modeling, constant phases  $\Delta\Phi = +90^\circ, +60^\circ, +30^\circ, 0^\circ, -30^\circ, -60^\circ, -90^\circ$  are considered and compared to experimental results. Strong screening of the applied perturbation is observed in the modeling of all  $\Delta\Phi$  configurations. Due to the small electron perpendicular flow in the inner plasma (Fig. 1(b)), small magnetic islands are observed on rational

surfaces  $q = 4/2, 5/2$  and  $6/2$ . In the pedestal, the electron perpendicular flow is however very large, giving rise to the shielding of magnetic perturbations [17], except at the very edge (normalized flux  $\psi_{norm} \geq 0.97$ ) where the large resistivity ( $\eta \propto T^{-3/2}$ ) allows for the formation of an ergodic layer, as observed in the Poincaré plot in Fig.1(a).

In experiments, for phases between  $+90^\circ$  and  $+60^\circ$ , the interaction between the applied RMP spectrum and the plasma induces a stronger ELM mitigation [11-12]. The plot of the magnetic flux perturbation on pedestal resonant surfaces (Fig.1(c)) as found in modeling shows that the  $+90^\circ / +60^\circ$  phases induce the maximum resonant response at the very edge (resonant surfaces  $q = m/n$  with  $m \geq 9$ , for  $\psi_{norm} \geq 0.97$ ). This corresponds to an optimal alignment of field lines with the magnetic perturbation, whereas the minimum perturbation on the edge resonant surfaces occurs for the opposite phase  $-90^\circ$  (field lines near perpendicular to perturbation). At the pedestal top ( $m = 7 - 8$ ), the amplitude is small in all cases, due to the strong shielding by electron perpendicular flow described above.

Poincaré plots for the two “extreme” configurations ( $\Delta\Phi = +90^\circ / -90^\circ$ ) are presented in Fig.2(a). The width of the ergodic layer is maximum for  $\Delta\Phi = +90^\circ$  (the magnetic field is ergodic for  $\psi_{norm} \geq 0.97$ ), consistently with the maximum resonant perturbation at the edge. On the contrary, the ergodic layer width is minimum for  $\Delta\Phi = -90^\circ$ . The Poincaré plot also highlights a maximum kinking of the field lines near the X-point in the most resonant case, while the kinking near the X-point is minimum in the least resonant case, but maximum at the midplane in this configuration. The Fourier spectrum of the magnetic flux perturbation  $\psi_{mn}$  shows that the field line kinking near the X-point is associated with the excitation of peeling-kink modes at the edge: modes  $m > nq$  in Fig.2(b, left). The observation of the peeling-kink amplification in this configuration is in good agreement with other modeling performed with MARS-F, VMEC and M3D-C1 [12,18-19]). The poloidal coupling between the kink modes  $m > nq$  and the resonant (tearing) mode  $m = nq$  (white diamonds in Fig.2(b)) at the edge induces the amplification of the resonant component, thus resulting in an enhanced ergodicity at the edge.

In addition, due to the breaking of the separatrix into stable and unstable manifolds [20] when RMPs are applied, the formation of typical lobe structures is observed near the X-point, inducing characteristic footprint patterns on divertor targets (Fig. 2(c)), responsible for the splitting of the strike points. The length of the footprints is clearly larger in the  $+90^\circ$  case, due to the stronger resonant response.

The displacement near the X-point is illustrated in Fig.2(d), where the density profile distribution is plotted versus  $Z$  and toroidal direction  $\phi$  in a vertical cut through the X-point. This excursion is maximum in the  $+90^\circ$  case ( $\Delta Z \approx 7\text{mm}$  on the turquoise  $q = 9/2$  surface) and minimum ( $\Delta Z \approx 2\text{mm}$ ) in the  $-90^\circ$  case. The distortion of the temperature profile follows a similar trend. At the outboard midplane, the displacement is maximum ( $\Delta R \approx 8\text{mm}$  on  $q = 9/2$ ) in the  $-90^\circ$  case and minimum in the resonant case ( $\Delta R \approx 3.5\text{mm}$ ), in qualitative agreements with the experimental ECEI measurements [21] and modeling performed with VMEC and MARS-F [12,18]. Note that other works show that there is a correlation between the X-point displacement and the strong ELM mitigation (due to the coupling between the peeling-kink and resonant components), however the midplane displacement can be either maximum or minimum in the most resonant configuration, depending on the q-profile [22].

Ergodicity and the large displacement of temperature and density near the X-point generate an increased radial heat and particle transport. In experiments, a maximum pumpout of density is observed in the most resonant case, resulting in a reduction of

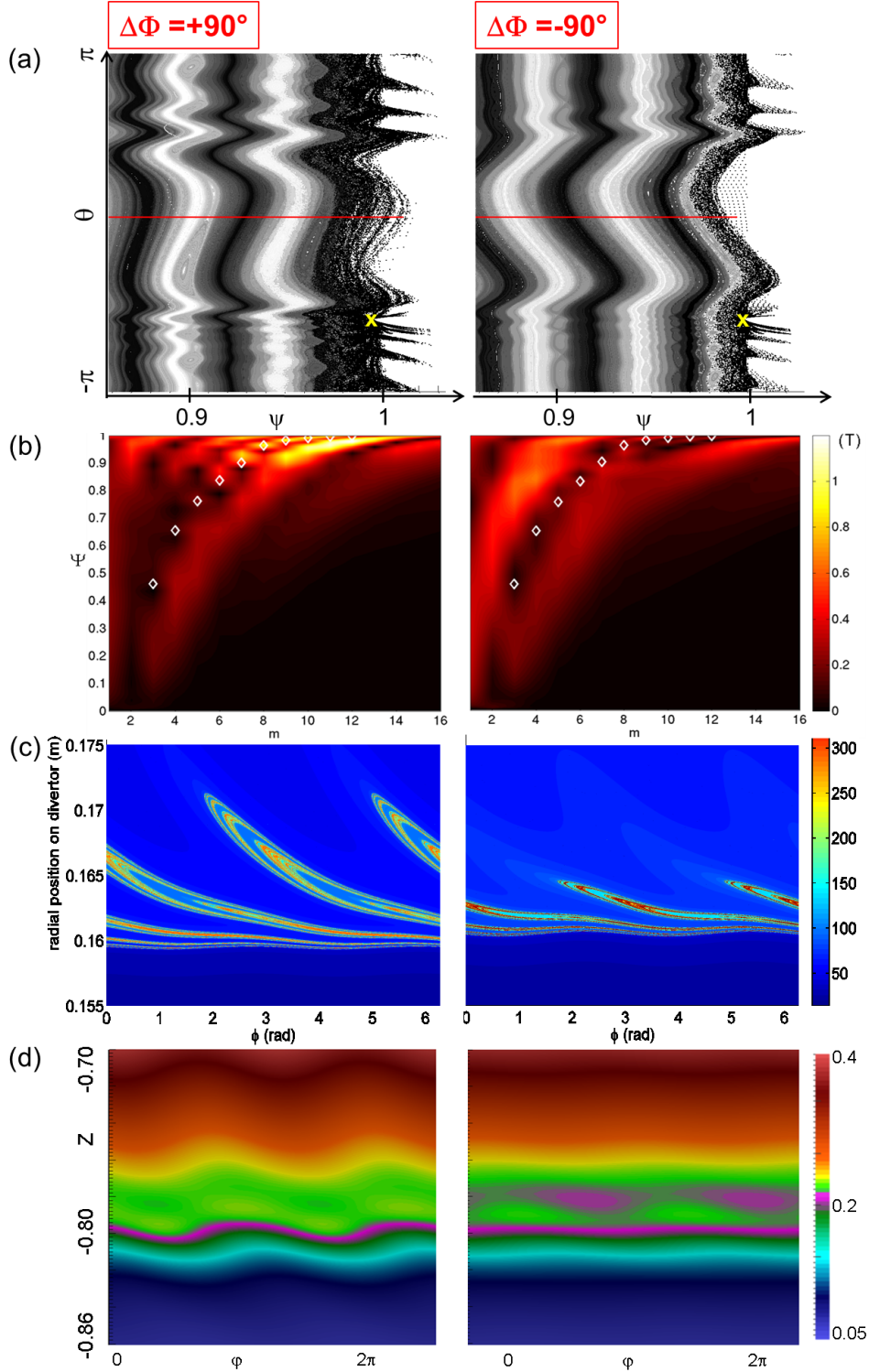


FIG. 2: For  $\Delta\Phi = +90^\circ$  (left) and  $-90^\circ$  (right): (a) Poincaré plot as a function of radial  $\psi_{norm}$  and poloidal  $\theta$  coordinates at the plasma edge. Midplane is represented by red lines and X-point by yellow crosses. (b) Fourier spectrum of the magnetic flux perturbation, as a function of the radial direction  $\psi_{norm}$  and the poloidal mode number  $m$ . Resonant surfaces  $q = m/2$  are marked with white diamonds. (c) Footprints induced by RMPs on divertor target: the connection length from target to target is plotted. (d) Displacement of the density profile in the toroidal direction at the vicinity of the X-point.

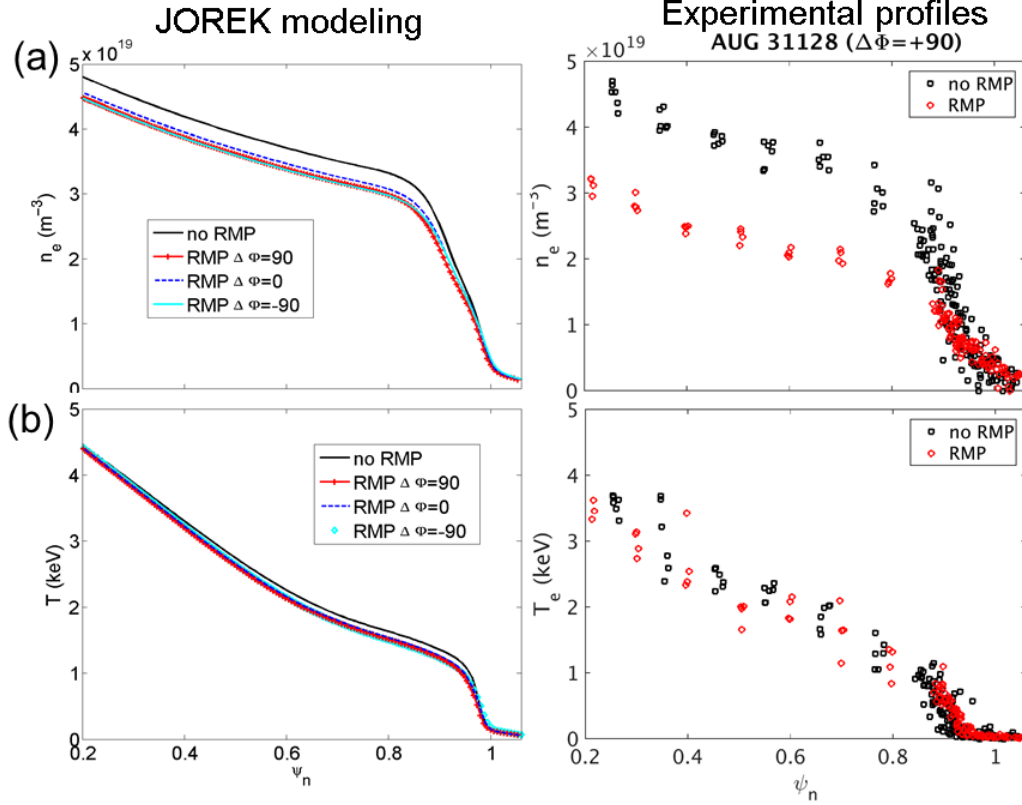


FIG. 3: Density (a) and electron temperature (b) profiles in modeling (left) as compared to experiments (right) in shot #31128 (for  $\Delta\Phi = +90^\circ$ )

density in the core plasma by  $\approx 30\%$  (as plotted in Fig.3(a), right), while the electron temperature profile (Fig.3(b), right) remains unaffected by RMP application. The time evolution of density and temperature profiles in modeling ( Fig.3, left) also shows a pumpout of density resulting in the degradation of the density profile. However the core density after RMP application is reduced by less than 10%. The modeled temperature profile is slightly degraded in the pedestal but remains constant in the core, in relatively good agreement with experimental observations. Therefore the increased particle and heat transport due to ergodicity partially explains the modification of the profiles, nevertheless other mechanisms may need to be considered to explain the large pumpout experimentally observed.

Another interesting feature that can be compared with experiments is the relation between the footprint pattern on divertor targets and the Infra-Red thermography measurements of the heat flux on divertor. Even though no IR data could be obtained in the shots considered above, precise IR data were obtained in L-mode discharges where the constant phase  $\Delta\Phi$  between applied coil currents is rotated in time. A different RMP spectrum is applied in different discharges, corresponding to a maximum resonant response at the edge in shot #32217 and a minimum edge resonance in shot #32218 [23-24], allowing us to validate the behaviour observed in modeling. In the first case, a clear  $n = 2$  heat flux pattern is measured in experiments (Fig.4(a, left)). The structure and radial extension of the footprint pattern on the divertor target found in modeling (Fig.4(b, left)) matches well the extension of the measured heat flux: the heat and particle transport follow the perturbed field lines. In the least resonant case (Fig.4(right)), the heat flux pattern is barely affected by RMPs: the small lobes found in modeling are in good agreement with experimental observations.

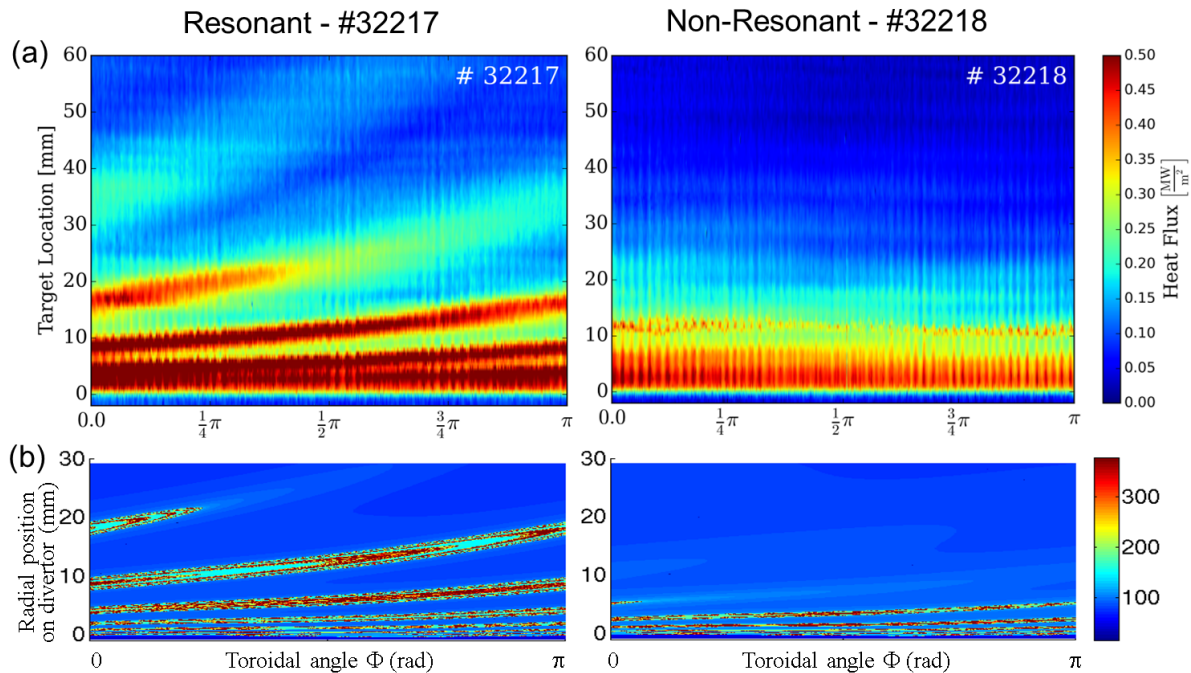


FIG. 4: In L-mode case, comparison of the Infra-Red thermography measurement of the heat flux on divertor (a) and modeling of the footprint on divertor (b), in shots where the applied perturbation maximize (left, shot #32217) or minimize (right, #32218) the resonant components at the edge.

### 3 Preliminary results of the interaction between ELMs and RMPs

As a second step, the interaction between ELMs and RMP fields is considered in multi-harmonic  $n$  simulations for the H-mode plasma described in the previous section. Without RMP, the most peeling-ballooning unstable mode is the  $n = 8$  mode, so modes up to  $n = 8$  were included in simulation; discarding the higher mode numbers allows us to reduce the computational cost of the simulations. The evolution of the coupling between modes is studied without RMP and with RMPs in the two most representative configurations  $\Delta\Phi = +90^\circ$  and  $-90^\circ$ .

Without RMP, unstable modes grow linearly and drive non-linearly the stable (low  $n$ ) modes as well [25], until all modes non-linearly saturate and the crash occurs. In this case, as plotted in Fig.5(a), the coupling between the most unstable modes  $n = 8$  and  $n = 7$  non-linearly drives the  $n = 1$  mode, then  $n = 8$  and  $n = 6$  drive the growth of  $n = 2$ , etc. At the ELM crash ( $t \approx 1.41\text{ms}$ ),  $n = 1, 2, 7$  and  $8$  are the dominant modes.

When RMPs are applied, the coupling between modes is modified, depending on the applied RMP spectrum. In the most resonant case ( $\Delta\Phi = +90^\circ$ ), the strong  $n = 2$  RMP perturbation drives all other even modes, while odd modes remain at a rather low level. In Fig.5(b), the growth rates of the  $n = 4$  mode is observed to be 2 times the one of the RMP  $n = 2$  mode (slowly ramped up in the simulation) and  $n = 8$  has a 4 times larger growth rate: it shows that the growth of the  $n = 4$  mode is essentially driven by quadratic products of  $n = 2$  terms and the  $n = 8$  mode is also driven by quadratic  $n = 4$  coupling as well as coupling between  $n = 2$  and  $n = 6$  (also driven by RMPs). The even

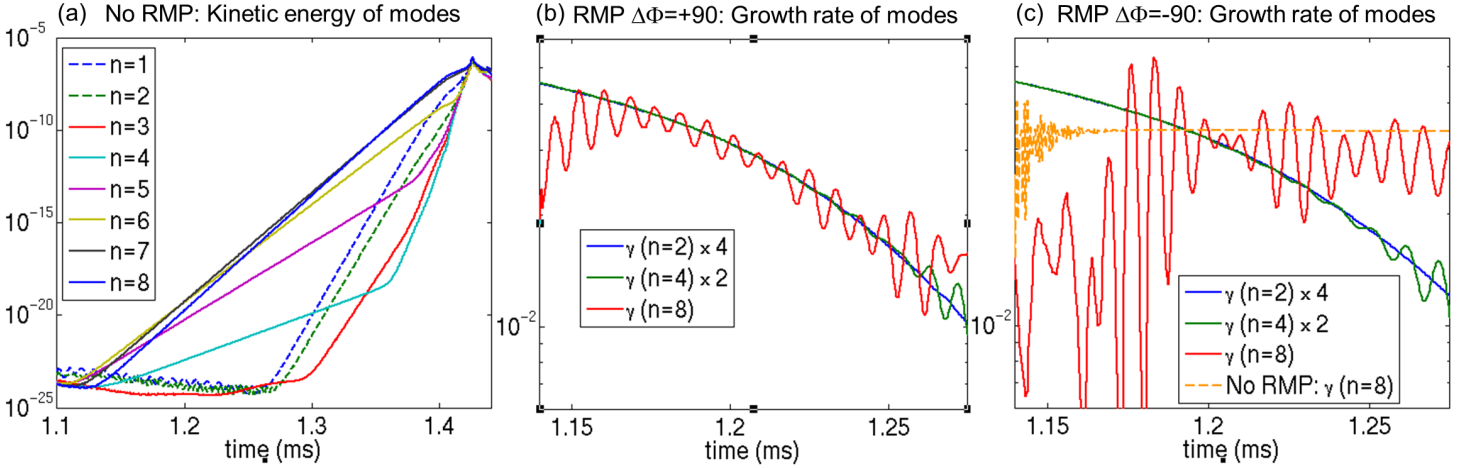


FIG. 5: Time evolution of: (a) Kinetic energy of toroidal modes  $n$  without RMPs. (b-c) With RMPs: Growth rate of modes  $n = 2$  ( $\times 4$ ),  $n = 4$  ( $\times 2$ ) and  $n = 8$  for  $\Delta\Phi = +90^\circ$  and  $-90^\circ$  respectively, showing a strong coupling of even modes with RMPs in the most resonant case as compared to no or weak coupling of  $n = 8$  mode in the least resonant case. In (c), the growth rate of  $n = 8$  without RMP is given in orange as comparison: with RMPs, the growth rate of  $n = 8$  is slightly lower than without RMP, due to the degraded pressure gradient when RMPs are applied.

modes are thus “constrained” by the RMP mode, preventing them to violently grow into a large ELM. However in the case where the edge kink and resonant responses are weakest ( $\Delta\Phi = -90^\circ$ , Fig.5(c)), the  $n = 2$  mode drives the dynamics of  $n = 4$ , whereas the  $n = 8$  mode is not coupled to  $n = 2$  RMPs and can grow linearly, leading to a larger ELM crash. The growth rate of the  $n = 8$  mode is slightly smaller than in the case without RMPs (in orange in Fig.5(c)), since the pedestal pressure gradient is reduced by RMPs, hence reducing the drive of the ELM. The observed oscillation corresponds to the diamagnetic frequency. This difference of coupling between modes in the two cases possibly explain why ELMs are strongly mitigated in experiments in the first case but not in the second case. These preliminary results will lead to a more detailed study.

## 4 Conclusion

The plasma response to RMPs and the interaction between ELMs and RMPs was studied with JOREK, trying to closely match the experimental observations. The RMP configuration for which the strongest ELM mitigation is obtained in experiments presents in modeling a maximum excitation of both the resonant and the edge-kink (or peeling) responses: the amplification of barely-stable kink modes induces a strengthened resonant component on rational surfaces at the edge due to poloidal mode coupling. Therefore enhanced ergodic layer, lobe patterns and 3D-displacement near the X-point are observed, in qualitative good agreement with experimental Electron Cyclotron Emission Imaging (ECEI) measurement of the displacement and IR thermography of the footprint patterns, as well as modeling with other codes (MARS-F, VMEC and M3D-C1). Density pumpout is induced in modeling due to ergodicity and 3D-displacement, however not as large as experimentally observed.

In the preliminary modeling of ELM-RMP interaction for the most and least resonant

RMP fields, a clear qualitative difference is observed in the behaviour of the  $n = 8$  mode which is linearly most unstable when no RMP fields are applied. In the most resonant case,  $n = 8$  is coupled to the  $n = 2$  external perturbation, driven entirely by the RMPs and does not show a ballooning mode structure. In contrast, in the weakly resonant case,  $n = 8$  is dominated by the linearly unstable ballooning mode with an only slightly lower growth rate compared to the no-RMP case (due to pedestal degradation). This difference may explain the experimental observation of stronger ELM mitigation in resonant cases, since a ballooning mode becoming unstable will be strongly influenced by a large RMP-driven background perturbation. This interaction may be very strong, since the perturbation non-linearly driven by RMPs has the same toroidal mode number as the ballooning mode. Detailed analysis of this mechanism is ongoing and will be described in more detail in future work.

## References

- [1] T. Evans *et al*, Phys. Rev. Lett. 92, 235003 (2004).
- [2] Y. Liang *et al*, Phys. Rev. Lett. 98, 265004 (2007).
- [3] J. Canik *et al*, Nucl. Fus. 50, 034012 (2010).
- [4] W. Suttrop *et al*, Phys. Rev. Lett. 106, 225004 (2011).
- [5] A. Kirk *et al*, Phys. Rev. Lett. 108, 255003 (2012).
- [6] Y. Jeon *et al* Phys. Rev. Lett. 109, 035004 (2012).
- [7] G. Huijsmans *et al*, Phys. Plas. 22, 02 1805 (2015).
- [8] Y. Liu *et al*, Nucl. Fus. 51, 083002 (2011).
- [9] M. Bécoulet *et al*, Phys. Rev. Lett. 113, 115001 (2014).
- [10] C. Paz-Soldan, R. Nazikian *et al*, Phys. Rev. Lett. 114, 105001 (2015).
- [11] A. Kirk *et al*, Nucl. Fus. 55, 043011 (2015).
- [12] W. Suttrop *et al*, PPCF 2016 submitted.
- [13] G. Huysmans *et al*, Nucl. Fus. 47, 659 (2007).
- [14] F. Orain *et al*, Phys. Plas. 20, 102510 (2013).
- [15] F. Orain *et al*, PPCF 2016 accepted.
- [16] E. Strumberger *et al*, Max-Planck-Institut für Plasmaphysik Laboratory Report IPP 5/112 (2005).
- [17] E. Nardon *et al*, Nucl. Fus. 50, 034002 (2010).
- [18] D. Ryan *et al*, PPCF 57, 095008 (2015).
- [19] B. Lyons *et al*, APS 2015.
- [20] P. Cahyna *et al*, IAEA 2013.
- [22] M. Willensdorfer *et al*, this conference, EXS/P6.
- [21] Y. Liu *et al*, Nucl. Fus. 56, 056015 (2016).
- [23] M. Faitsch *et al*, JNM 2016 submitted.
- [24] B. Sieglin *et al*, this conference, EX/7-3Ra.
- [25] I. Krebs *et al*, Phys. Plas. 20, 082506 (2013).

**Acknowledgement:** This work has been carried out within the framework of the EUROfusion Consortium and has received funding from the Euratom research and training programme 2014-2018 under grant agreement No 633053. The work of Pavel Cahyna was partly supported by the Czech Science Foundation grant GA16-24724S. Part of this work was carried out using the HELIOS supercomputer system at Computational Situational Centre of International Fusion Energy Research Centre (IFERC-CSC), Aomori, Japan, under the Broader Approach collaboration between Euratom and Japan, implemented by Fusion for Energy and JAEA. The views and opinions expressed herein do not necessarily reflect those of the European Commission.